PIVOTING FACTORIZATION: A COMPACT META LOW-RANK REPRESENTATION OF SPARSITY FOR EFFICIENT INFERENCE IN LARGE LANGUAGE MODELS

Jialin Zhao[1,2], **Yingtao Zhang**[1,2], **Carlo Vittorio Cannistraci**[1,2,3] *
[1]Center for Complex Network Intelligence, Tsinghua Laboratory of Brain and Intelligence
[2]Department of Computer Science
[3]Department of Biomedical Engineering, Tsinghua University, Beijing, China

ABSTRACT

The rapid growth of Large Language Models has driven demand for effective model compression techniques to reduce memory and computation costs. Low-rank pruning has gained attention for its tensor coherence and GPU compatibility across all densities. However, low-rank pruning has struggled to match the performance of semi-structured pruning, often doubling perplexity (PPL) at similar densities. In this paper, we propose Pivoting Factorization (**PIFA**), a novel **lossless** meta low-rank representation that unsupervisedly learns a compact form of any low-rank representation, effectively eliminating redundant information. PIFA identifies pivot rows (linearly independent rows) and expresses non-pivot rows as linear combinations, achieving an additional **24.2%** memory savings and **24.6%** faster inference over low-rank layers at $r/d = 0.5$, thereby significantly enhancing performance at the same density. To mitigate the performance degradation caused by low-rank pruning, we introduce a novel, retraining-free low-rank reconstruction method that minimizes error accumulation (**M**). **MPIFA**, combining M and PIFA into an end-to-end framework, significantly outperforms existing low-rank pruning methods and, for the first time, achieves performance comparable to semi-structured pruning, while surpassing it in GPU efficiency and compatibility.

1 INTRODUCTION

The rapid growth of Large Language Models (LLMs) (Radford, 2018; Radford et al., 2019; Mann et al., 2020; Touvron et al., 2023a) has driven demand for efficient model compression to address memory and computation costs (Wan et al., 2023; Zhu et al., 2024). Among these techniques, *semi-structured pruning*, specifically N:M sparsity, enables hardware-friendly acceleration on NVIDIA's Ampere GPUs (Mishra et al., 2021; nvi, 2020) but lacks flexibility in adjusting density, and restricted to specific hardware architectures. Conversely, *low-rank pruning*, based on Singular Value Decomposition (SVD), maintains GPU compatibility at any density (Hsu et al., 2022; Yuan et al., 2023; Wang et al., 2024). However, it struggles to match semi-structured pruning in performance, often resulting in a **2x increase in perplexity** at the same densities due to (1) **information redundancy** in decomposed weight matrices and (2) **error accumulation** across layers.

To address challenge (1), we propose **Pivoting Factorization (PIFA)**, a lossless meta low-rank representation that compresses existing low-rank decompositions. PIFA selects r pivot rows (linearly independent rows) and expresses all others as their linear combinations, achieving **24.2%** memory savings and **24.6%** faster inference over low-rank layers at $r/d = 0.5$, **without inducing any loss**.

To address challenge (2), we propose an **Online Error-Accumulation-Minimization Reconstruction (M)** algorithm, which mitigates errors propagated through reconstruction in low-rank (Wang et al., 2024) and semi-structured pruning (Frantar & Alistarh, 2023; Li et al., 2024). Existing methods rely on **degraded data flow**, leading to suboptimal performance. M corrects accumulated errors by integrating dense and low-rank data flows as reconstruction targets.

*Correspondence to: Jialin Zhao <jialin.zhao97@gmail.com>, Carlo Vittorio Cannistraci <kaloka-gathos.agon@gmail.com>.

Table 1: **Comparison of PIFA with other sparsity.**

Method	CPU Speedup	GPU Speedup	GPU Mem Reduction	Any Sparsity	GPU Support	Performance
Unstructured Sparsity	✓	✗	✗	✓	✗	✓✓✓
Semi-Structured Sparsity	✓	✓	✓	✗	Ampere GPU	✓✓
Structured Sparsity	✓	✓	✓	✓	General	✓
SVD-Based Low-Rank Sparsity	✓	✓	✓	✓	General	✓
PIFA Low-Rank Sparsity	✓	✓	✓	✓	General	✓✓

Figure 1: **Comparison of parameter ratios**.

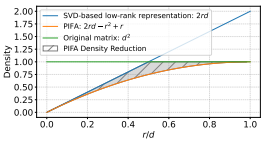

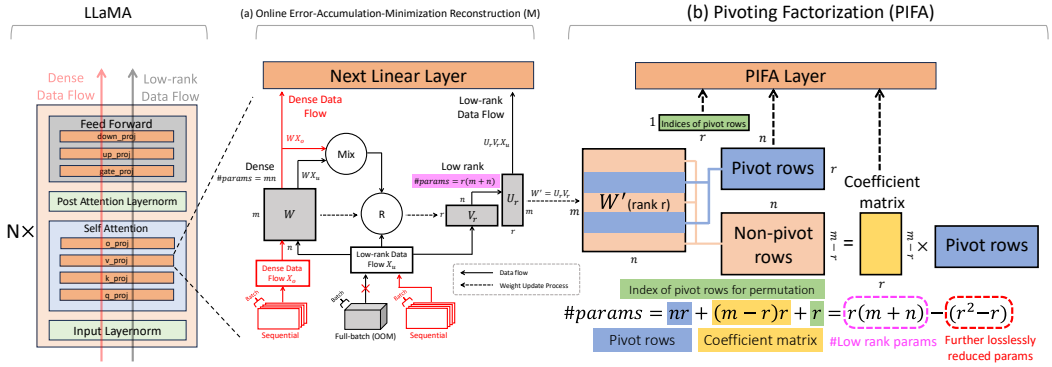

Figure 2: Illustration of the low-rank pruning method **MPIFA** (Algorithm 3), which consists of: **(a) Online Error-Accumulation-Minimization Reconstruction (M)**. Block R solves the least-squares optimization problem. The improvements upon SVD-LLM's full-batch reconstruction, highlighted in red, include using the dense data flow to minimize error accumulation, and processing each sample sequentially to avoid GPU memory overflow. **(b) Pivoting Factorization (PIFA)**. For **any singular matrix** with rank r, Pivoting Factorization further reduces $r^2 - r$ parameters, with no additional loss induced.

Combining M and PIFA, we introduce **MPIFA**, an end-to-end, retraining-free low-rank pruning framework that reduces the perplexity gap by **40%-70%** on LLaMA2 and LLaMA3, compared with existing low-rank pruning methods. MPIFA achieves **superior** speedup and memory savings over *semi-structured pruning* while maintaining **comparable** or better perplexity. At $d = 32768$, PIFA with 55% density achieves a **2.1**× speedup, whereas semi-sparse implementations are slower or fail to execute (Table 4). Related work is included in Appendix J.

2 Lossless Low-Rank Compression

2.1 Motivation: Information Redundancy in Singular Value Decomposition

Low-rank pruning (Hsu et al., 2022; Yuan et al., 2023; Wang et al., 2024) approximates a weight matrix $\mathbf{W} \in \mathbb{R}^{m\times n}$ as $\mathbf{W} \approx \mathbf{U}\mathbf{V}^{\mathrm{T}}$, where $\mathbf{U} \in \mathbb{R}^{m\times r}$ and $\mathbf{V}^{\mathrm{T}} \in \mathbb{R}^{r\times n}$.

This representation has $r(m+n)$ parameters. When r exceeds half of the matrix dimensions, low-rank compression fails to achieve compression (Figure 1). But orthogonality constraints among singular vectors reduce the effective degrees of freedom by $r(r-1)$, leading to redundancy.

> ***Question:*** Can we design a matrix factorization method that reduces parameters to $r(m+n)-(r^2-r)$ without losing representational power?

2.2 Pivoting Factorization

To address the redundancy in low-rank decompositions, we propose **Pi**voting **Fa**ctorization (**PIFA**), a novel matrix factorization method that further reduces parameters without additional loss.

As illustrated in Figure 2(b), given a low-rank decomposition $\mathbf{U} \in \mathbb{R}^{m\times r}$ and $\mathbf{V}^{\mathrm{T}} \in \mathbb{R}^{r\times n}$, we first reconstruct $\mathbf{W}' = \mathbf{U}\mathbf{V}^{\mathrm{T}}$. Since $\mathbf{W}'$ has rank r, it contains r linearly independent pivot rows, identified via LU or QR decomposition with pivoting (Businger & Golub, 1971). Let $\mathcal{I}$ denote their

indices, and $\mathcal{I}^c$ the remaining non-pivot rows. Then, we define:

$$\mathbf{W}_p = \mathbf{W}'[\mathcal{I}, :], \quad \mathbf{W}_{np} = \mathbf{W}'[\mathcal{I}^c, :] \tag{1}$$

where $\mathbf{W}_p \in \mathbb{R}^{r \times n}$ is the pivot-row matrix, and $\mathbf{W}_{np} \in \mathbb{R}^{(m-r) \times n}$ is the non-pivot-row matrix. Non-pivot-row matrix can be expressed as a linear combination of pivot rows:

$$\mathbf{W}_{np} = \mathbf{C}\mathbf{W}_p \tag{2}$$

where $\mathbf{C} \in \mathbb{R}^{(m-r) \times r}$ is the coefficient matrix. Algorithm 1 details the PIFA process, which generates the components of a PIFA layer: pivot-row indices $\mathcal{I}$, the pivot-row matrix $\mathbf{W}_p$, and the coefficient matrix $\mathbf{C}$. This further losslessly reduces $r^2 - r$ parameters, compared with low-rank layer. Algorithm 2 describes the inference procedure for the PIFA layer, which leverages $\mathbf{W}_p$, $\mathbf{C}$ and $\mathcal{I}$ to compute the output. The analysis of memory and computational cost of PIFA is included in Appendix A, in which we demonstrate that PIFA consistently requires less memory and computational cost than low-rank layer and dense linear layer.

3 Online Error-Accumulation-Minimization Reconstruction

SVD-LLM (Wang et al., 2024) introduced low-rank matrix reconstruction by updating $\mathbf{U}$ via a closed-form least squares solution:

$$\mathbf{U}_r = \arg\min_{\mathbf{U}} \|\mathbf{W}\mathbf{X} - \mathbf{U}\mathbf{V}^{\mathrm{T}}\mathbf{X}\|_{\mathrm{F}} \tag{3}$$

where $\mathbf{X}$ is the calibration data. We propose **Online Error-Accumulation-Minimization Reconstruction (M)**, addressing error accumulation in low-rank pruning (Wang et al., 2024) and semi-structured pruning (Frantar & Alistarh, 2023; Li et al., 2024). These methods rely solely on one data flow, i.e. low-rank data flow in Figure 2. This approach allows accumulated errors from previous modules to propagate through the reconstruction process, potentially degrading performance, as each subsequent module is optimized based on an already-degraded data flow.

To mitigate this, our method corrects accumulated errors at each module by aligning reconstruction with the dense data flow:

$$\min \|\mathbf{W}\mathbf{X}_o - \mathbf{U}\mathbf{V}^{\mathrm{T}}\mathbf{X}_u\|_{\mathrm{F}} \tag{4}$$

where $\mathbf{X}_o$ and $\mathbf{X}_u$ represent inputs from dense and low-rank weights, respectively. This realignment ensures that each module's output remains aligned with the output of original model, recovering the accumulated error in $\mathbf{X}_u$.

However, solely relying on the dense data flow risks overfitting to calibration data. Instead, we use a weighted mix of dense and low-rank data flow:

$$\mathbf{Y}_t = \lambda\mathbf{W}\mathbf{X}_o + (1-\lambda)\mathbf{W}\mathbf{X}_u \tag{5}$$

where λ is the **mix ratio**. The optimization target becomes $\min \|\mathbf{Y}_t - \mathbf{U}\mathbf{V}^{\mathrm{T}}\mathbf{X}_u\|_{\mathrm{F}}$. The low-rank output acts as a regularization term, improving generalization and preventing overfitting. Empirically, $\lambda = 0.25$ provides the best balance (see Appendix G).

Further improvements, including the online least squares formulation and reconstruction of $\mathbf{V}^{\mathrm{T}}$, are detailed in Appendices B and C.

4 Experiments

4.1 Main Result

Experimental details are provided in Appendix E, with fine-tuning results in Appendix E.6 and ablation studies in Appendix G.

Comparison with other low-rank pruning. Table 2 displays the test perplexity (PPL) of each low-rank pruning method on WikiText2 under 0.4-0.9 density. The results show that MPIFA significantly outperforms other low-rank pruning method, reducing the perplexity gap by **66.4%** (LLaMA2-7B), **53.8%** (LLaMA2-13B), **40.7%** (LLaMA2-70B), and **72.7%** (LLaMA3-8B) on average.

Table 2: **Perplexity (↓) at different parameter density** (proportion of remaining parameters relative to the original model) on WikiText2. The best-performing method is highlighted in **bold**.

		Density						
Model	Method	100%	90%	80%	70%	60%	50%	40%
LLaMA2-7B	SVD	5.47	16063	18236	30588	39632	53179	65072
	ASVD		5.91	9.53	221.6	5401	26040	24178
	SVD-LLM		7.27	8.38	10.66	16.11	27.19	54.20
	MPIFA		**5.69**	**6.16**	**7.05**	**8.81**	**12.77**	**21.25**
LLaMA2-13B	SVD	4.88	2168	6177	37827	24149	14349	41758
	ASVD		5.12	6.67	17.03	587.1	3103	4197
	SVD-LLM		5.94	6.66	8.00	10.79	18.38	42.79
	MPIFA		**5.03**	**5.39**	**7.12**	**7.41**	**10.30**	**16.72**
LLaMA2-70B	SVD	3.32	6.77	17.70	203.7	2218	6803	15856
	ASVD		OOM	OOM	OOM	OOM	OOM	OOM
	SVD-LLM		4.12	4.58	5.31	6.60	9.09	14.82
	MPIFA		**3.54**	**3.96**	**4.58**	**5.54**	**7.40**	**12.01**
LLaMA3-8B	SVD	6.14	463461	626967	154679	62640	144064	216552
	ASVD		9.37	275.6	12553	21756	185265	13504
	SVD-LLM		9.83	13.62	23.66	42.60	83.46	163.5
	MPIFA		**6.93**	**8.31**	**10.83**	**16.41**	**28.90**	**47.02**

Table 3: **Perplexity (↓) comparison with semi-structured pruning** under the same memory reduction on WikiText2. MPIFA_{NS} means MPIFA using non-uniform sparsity.

Method	LLaMA2-7B	LLaMA2-13B
Dense	5.47	4.88
Magnitude 2:4	37.77	8.89
Wanda 2:4	11.40	8.33
RIA 2:4	10.85	8.03
SVD 55%	69128	24947
ASVD 55%	9370	2039
SVD-LLM 55%	20.43	13.69
MPIFA_{NS} 55%	**9.68**	**7.93**

Figure 3: **Layerwise speedup of PIFA and semi-sparse layers** in FP16 (FP32 unsupported for 2:4 sparsity in `torch.sparse`). PIFA's speedup increases with dimension.

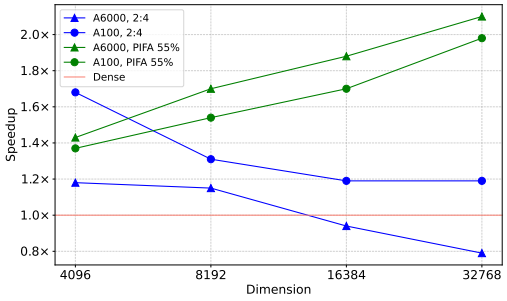

Comparison with semi-structured pruning. Table 3 shows that MPIFA_{NS} outperforms 2:4 pruning methods, reducing the perplexity gap by **21.7%** for LLaMA2-7B and **3.2%** for LLaMA2-13B.

4.2 Inference Speedup and Memory Reduction

PIFA layer vs low-rank layer. The PIFA layer achieves significant savings in both memory and computation time, as shown in Figure 4, PIFA losslessly compresses the memory of the low-rank layer by 24.2% and reduces inference time by 24.6%.

PIFA layer vs semi-sparse layer. Figure 3 and Table 4 compare the speedup and memory usage of PIFA and 2:4 semi-sparse layers (cuSPARSELt and CUTLASS) across various dimensions on A6000 and A100 GPUs. PIFA demonstrates consistently superior efficiency, achieving the highest speedup and lowest memory usage in all cases except $d = 4096$. Notably, PIFA's acceleration increases with matrix dimensions, reflecting its scalability and computational effectiveness. End-to-end LLM inference comparison is provided in Appendix F.

5 Conclusion

We propose **MPIFA**, a retraining-free low-rank pruning framework that integrates **Pivoting Factorization (PIFA)** and **Online Error-Accumulation-Minimization Reconstruction (M)**. PIFA enhances memory savings and inference speedup, while M mitigates error accumulation for improved performance. Future work could explore integrating PIFA into pretraining to further enhance model efficiency.

REFERENCES

Nvidia a100 tensor core gpu architecture, 2020. URL https://www.nvidia.com/content/dam/en-zz/Solutions/Data-Center/nvidia-ampere-architecture-whitepaper.pdf. Accessed: 2025-01-29.

From galore to welore: Memory-efficient finetuning with adaptive low-rank weight projection. *arXiv preprint arXiv:2310.01382*, 2024.

Saleh Ashkboos, Maximilian L. Croci, Marcelo Gennari do Nascimento, Torsten Hoefler, and James Hensman. SliceGPT: Compress large language models by deleting rows and columns. In *The Twelfth International Conference on Learning Representations*, 2024. URL https://openreview.net/forum?id=vXxardq6db.

P Businger and GH Golub. Linear least squares solutions by householder transformations. *Handbook for automatic computation*, 2:111–118, 1971.

Rocktim Jyoti Das, Mingjie Sun, Liqun Ma, and Zhiqiang Shen. Beyond size: How gradients shape pruning decisions in large language models, 2024. URL https://arxiv.org/abs/2311.04902.

Peijie Dong, Lujun Li, Zhenheng Tang, Xiang Liu, Xinglin Pan, Qiang Wang, and Xiaowen Chu. Pruner-zero: Evolving symbolic pruning metric from scratch for large language models. In *Forty-first International Conference on Machine Learning*, 2024. URL https://openreview.net/forum?id=1tRLxQzdep.

Abhimanyu Dubey, Abhinav Jauhri, Abhinav Pandey, Abhishek Kadian, Ahmad Al-Dahle, Aiesha Letman, Akhil Mathur, Alan Schelten, Amy Yang, Angela Fan, et al. The llama 3 herd of models. *arXiv preprint arXiv:2407.21783*, 2024.

Gongfan Fang, Hongxu Yin, Saurav Muralidharan, Greg Heinrich, Jeff Pool, Jan Kautz, Pavlo Molchanov, and Xinchao Wang. MaskLLM: Learnable semi-structured sparsity for large language models. In *The Thirty-eighth Annual Conference on Neural Information Processing Systems*, 2024. URL https://openreview.net/forum?id=Llu9nJal7b.

Elias Frantar and Dan Alistarh. Sparsegpt: Massive language models can be accurately pruned in one-shot. In *International Conference on Machine Learning*, pp. 10323–10337. PMLR, 2023.

Leo Gao, Jonathan Tow, Stella Biderman, Sid Black, Anthony DiPofi, Charles Foster, Laurence Golding, Jeffrey Hsu, Kyle McDonell, Niklas Muennighoff, Jason Phang, Laria Reynolds, Eric Tang, Anish Thite, Ben Wang, Kevin Wang, and Andy Zou. A framework for few-shot language model evaluation, September 2021. URL https://doi.org/10.5281/zenodo.5371628.

Babak Hassibi, David G Stork, and Gregory J Wolff. Optimal brain surgeon and general network pruning. In *IEEE international conference on neural networks*, pp. 293–299. IEEE, 1993.

Yen-Chang Hsu, Ting Hua, Sungen Chang, Qian Lou, Yilin Shen, and Hongxia Jin. Language model compression with weighted low-rank factorization. In *International Conference on Learning Representations*, 2022. URL https://openreview.net/forum?id=uPv9Y3gmAI5.

Yann Le Cun, JS Denker, and SA Solla. Optimal brain damage, advances in neural information processing systems. *Denver 1989, Ed. D. Touretzsky, Morgan Kaufmann*, 598:605, 1990.

Guanchen Li, Xiandong Zhao, Lian Liu, Zeping Li, Dong Li, Lu Tian, Jie He, Ashish Sirasao, and Emad Barsoum. Enhancing one-shot pruned pre-trained language models through sparse-dense-sparse mechanism, 2024. URL https://arxiv.org/abs/2408.10473.

Chi-Heng Lin, Shangqian Gao, James Seale Smith, Abhishek Patel, Shikhar Tuli, Yilin Shen, Hongxia Jin, and Yen-Chang Hsu. Modegpt: Modular decomposition for large language model compression, 2024. URL https://arxiv.org/abs/2408.09632.

Haiquan Lu, Yefan Zhou, Shiwei Liu, Zhangyang Wang, Michael W. Mahoney, and Yaoqing Yang. Alphapruning: Using heavy-tailed self regularization theory for improved layer-wise pruning of large language models. In *The Thirty-eighth Annual Conference on Neural Information Processing Systems*, 2024. URL https://openreview.net/forum?id=fHq4x2YXVv.

Xinyin Ma, Gongfan Fang, and Xinchao Wang. Llm-pruner: On the structural pruning of large language models. In *Advances in Neural Information Processing Systems*, 2023.

Ben Mann, N Ryder, M Subbiah, J Kaplan, P Dhariwal, A Neelakantan, P Shyam, G Sastry, A Askell, S Agarwal, et al. Language models are few-shot learners. *arXiv preprint arXiv:2005.14165*, 1, 2020.

Stephen Merity, Caiming Xiong, James Bradbury, and Richard Socher. Pointer sentinel mixture models. In *International Conference on Learning Representations*, 2022.

Asit Mishra, Jorge Albericio Latorre, Jeff Pool, Darko Stosic, Dusan Stosic, Ganesh Venkatesh, Chong Yu, and Paulius Micikevicius. Accelerating sparse deep neural networks. *arXiv preprint arXiv:2104.08378*, 2021.

Decebal Constantin Mocanu, Elena Mocanu, Peter Stone, Phuong H Nguyen, Madeleine Gibescu, and Antonio Liotta. Scalable training of artificial neural networks with adaptive sparse connectivity inspired by network science. *Nature communications*, 9(1):2383, 2018.

Alec Radford. Improving language understanding by generative pre-training. 2018.

Alec Radford, Jeffrey Wu, Rewon Child, David Luan, Dario Amodei, Ilya Sutskever, et al. Language models are unsupervised multitask learners. *OpenAI blog*, 1(8):9, 2019.

Colin Raffel, Noam Shazeer, Adam Roberts, Katherine Lee, Sharan Narang, Michael Matena, Yanqi Zhou, Wei Li, and Peter J. Liu. Exploring the limits of transfer learning with a unified text-to-text transformer. *J. Mach. Learn. Res.*, 21(1), January 2020. ISSN 1532-4435.

Mingjie Sun, Zhuang Liu, Anna Bair, and J Zico Kolter. A simple and effective pruning approach for large language models. In *The Twelfth International Conference on Learning Representations*, 2024. URL https://openreview.net/forum?id=PxoFut3dWW.

Hugo Touvron, Thibaut Lavril, Gautier Izacard, Xavier Martinet, Marie-Anne Lachaux, Timothée Lacroix, Baptiste Rozière, Naman Goyal, Eric Hambro, Faisal Azhar, et al. Llama: Open and efficient foundation language models. *arXiv preprint arXiv:2302.13971*, 2023a.

Hugo Touvron, Louis Martin, Kevin Stone, Peter Albert, Amjad Almahairi, Yasmine Babaei, Nikolay Bashlykov, Soumya Batra, Prajjwal Bhargava, Shruti Bhosale, et al. Llama 2: Open foundation and fine-tuned chat models. *arXiv preprint arXiv:2307.09288*, 2023b.

Tycho F. A. van der Ouderaa, Markus Nagel, Mart Van Baalen, and Tijmen Blankevoort. The LLM surgeon. In *The Twelfth International Conference on Learning Representations*, 2024. URL https://openreview.net/forum?id=DYIIRgwg2i.

Zhongwei Wan, Xin Wang, Che Liu, Samiul Alam, Yu Zheng, Jiachen Liu, Zhongnan Qu, Shen Yan, Yi Zhu, Quanlu Zhang, et al. Efficient large language models: A survey. *arXiv preprint arXiv:2312.03863*, 2023.

Xin Wang, Yu Zheng, Zhongwei Wan, and Mi Zhang. Svd-llm: Truncation-aware singular value decomposition for large language model compression. *arXiv preprint arXiv:2403.07378*, 2024.

Mao Ye, Chengyue Gong, Lizhen Nie, Denny Zhou, Adam Klivans, and Qiang Liu. Good subnetworks provably exist: Pruning via greedy forward selection. In *International Conference on Machine Learning*, pp. 10820–10830. PMLR, 2020.

Lu Yin, You Wu, Zhenyu Zhang, Cheng-Yu Hsieh, Yaqing Wang, Yiling Jia, Gen Li, AJAY KUMAR JAISWAL, Mykola Pechenizkiy, Yi Liang, et al. Outlier weighed layerwise sparsity (owl): A missing secret sauce for pruning llms to high sparsity. In *Forty-first International Conference on Machine Learning*.

Zhihang Yuan, Yuzhang Shang, Yue Song, Qiang Wu, Yan Yan, and Guangyu Sun. Asvd: Activation-aware singular value decomposition for compressing large language models. *arXiv preprint arXiv:2312.05821*, 2023.

Yingtao Zhang, Haoli Bai, Haokun Lin, Jialin Zhao, Lu Hou, and Carlo Vittorio Cannistraci. Plug-and-play: An efficient post-training pruning method for large language models. In *The Twelfth International Conference on Learning Representations*, 2024. URL https://openreview.net/forum?id=Tr0lPx9woF.

Michael Zhu and Suyog Gupta. To prune, or not to prune: exploring the efficacy of pruning for model compression. *arXiv preprint arXiv:1710.01878*, 2017.

Xunyu Zhu, Jian Li, Yong Liu, Can Ma, and Weiping Wang. A survey on model compression for large language models. *Transactions of the Association for Computational Linguistics*, 12:1556–1577, 2024.

Zhuangwei Zhuang, Mingkui Tan, Bohan Zhuang, Jing Liu, Yong Guo, Qingyao Wu, Junzhou Huang, and Jinhui Zhu. Discrimination-aware channel pruning for deep neural networks. *Advances in neural information processing systems*, 31, 2018.

Algorithm 1 Pivoting Factorization

input Low-rank matrix $\mathbf{W}' \in \mathbb{R}^{m \times n}$ with rank r

1: Use QR (or LU) decomposition with pivoting to find pivot-row indices: $\mathcal{I} \leftarrow \mathrm{QR}_{\mathrm{pivot}}(\mathbf{W}')$
2: Define $\mathcal{I}^c = \{1, 2, \ldots, m\} \setminus \mathcal{I}$, the complement of $\mathcal{I}$, representing non-pivot row indices
3: Compute pivot-row matrix: $\mathbf{W}_p \leftarrow \mathbf{W}'[\mathcal{I}, :]$
4: Compute non-pivot-row matrix: $\mathbf{W}_{np} \leftarrow \mathbf{W}'[\mathcal{I}^c, :]$
5: Compute coefficient matrix $\mathbf{C}$ by solving matrix equation: $\mathbf{C} \leftarrow \mathrm{linsolve}(\mathbf{W}_{np} = \mathbf{C}\mathbf{W}_p)$

output PIFA layer P: 1) Pivot-row indices $\mathcal{I} \in \mathbb{R}^r$; 2) pivot-row matrix $\mathbf{W}_p \in \mathbb{R}^{r \times n}$; 3) coefficient matrix $\mathbf{C} \in \mathbb{R}^{(m-r) \times r}$ for non-pivot rows

Algorithm 2 PIFA Layer

input Input $\mathbf{X} \in \mathbb{R}^{n \times b}$, where b is batch size; pivot-row indices $\mathcal{I} \in \mathbb{R}^r$; pivot-row matrix $\mathbf{W}_p \in \mathbb{R}^{r \times n}$; coefficient matrix $\mathbf{C} \in \mathbb{R}^{(m-r) \times r}$ for non-pivot rows

1: Define $\mathcal{I}^c = \{1, 2, \ldots, m\} \setminus \mathcal{I}$ representing non-pivot row indices
2: Compute output of pivot channels: $\mathbf{Y}_p \leftarrow \mathbf{W}_p\mathbf{X}$
3: Compute output of non-pivot channels: $\mathbf{Y}_{np} \leftarrow \mathbf{C}\mathbf{Y}_p$
4: Assign pivot channels to output: $\mathbf{Y}[\mathcal{I}, :] \leftarrow \mathbf{Y}_p$
5: Assign non-pivot channels to output: $\mathbf{Y}[\mathcal{I}^c, :] \leftarrow \mathbf{Y}_{np}$

output $\mathbf{Y}$

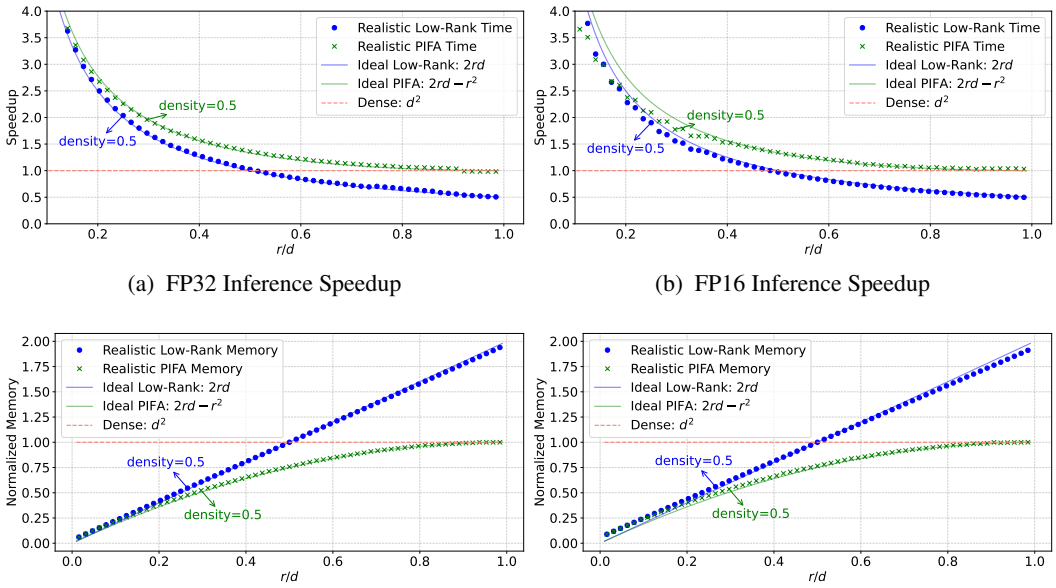

(a) FP32 Inference Speedup

(b) FP16 Inference Speedup

(c) FP32 Inference Memory

(d) FP16 Inference Memory

Figure 4: **Efficiency of PIFA layer** under various ranks, with sequence length = 2048, batch size = 32, and dimension = 8192 on FP32 and FP16 on A6000 GPU. At 50% density, PIFA achieves 47.6% memory savings and $1.95\times$ speedup on FP32. These results guarantee that the overhead of both time and memory of the PIFA layer is quite low.

Table 4: **Efficiency of PIFA layer and semi-sparse layer** across different dimensions, compared to dense linear at same dimension on same GPU, with sequence length of 2048 and batch size of 32, using FP16 (FP32 is not supported by 2:4 sparsity in `torch.sparse`). The highest speedup and lowest memory are indicated in **bold**. PIFA shows increasing speedup as the dimension grows. †For matrix multiplication with weight matrix shape 32768×32768, cuSPARSELt raises CUDA error.

			Dimension			
	GPU	Kernel	32768	16384	8192	4096
Speedup	A6000	2:4 (cuSPARSELt)	Error†	0.94×	0.97×	1.09×
		2:4 (CUTLASS)	0.79×	0.92×	1.15×	1.18×
		PIFA 55%	**2.10**×	**1.88**×	**1.70**×	**1.43**×
	A100	2:4 (cuSPARSELt)	Error†	1.19×	1.31×	**1.68**×
		2:4 (CUTLASS)	1.19×	1.12×	1.09×	1.52×
		PIFA 55%	**1.98**×	**1.70**×	**1.54**×	1.37×
Memory	2:4 (cuSPARSELt / CUTLASS)		0.564	0.569	0.589	0.651
	PIFA 55%		**0.552**	**0.558**	**0.578**	**0.645**

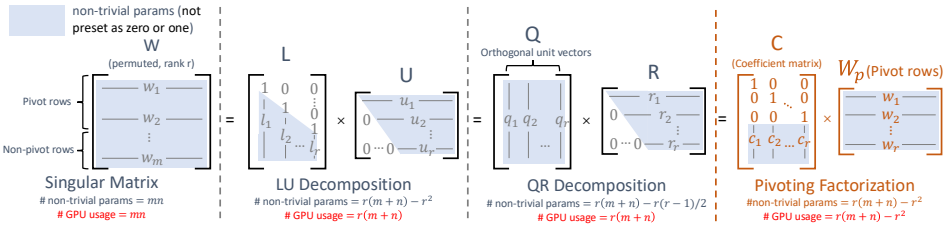

Figure 5: **Pivoting Factorization vs. LU and QR decompositions.** Applied to the permuted matrix (pivot rows at the top), Pivoting Factorization avoids the trapezoidal distribution of non-trivial parameters in LU decomposition, instead reorganizing them into a rectangular pattern. This structure optimizes GPU memory usage and reduces computation overhead.

A Memory and Computational Cost of PIFA

Memory cost of PIFA. For each low-rank weight matrix $\mathbf{W}'$, PIFA needs to store $\mathcal{I}$, $\mathbf{W}_p$ and $\mathbf{C}$, totaling $r(m+n) - r^2 + r$. Figure 1 illustrates the relationship between the number of parameters in PIFA, traditional low-rank decomposition, and a dense weight matrix (square).

Since $r(m+n) > r(m+n) - r^2 + r$ for any rank r, PIFA consistently requires less memory than traditional low-rank decomposition. For the comparison with dense weight matrix, because $r < \min(m, n)$, we have:

$$(m-r)(n-r) > 0 \quad \Rightarrow \quad mn > r(m+n) - r^2 \tag{6}$$

Neglecting the pivot-row index $\mathcal{I}$, which has negligible memory overhead compared to other variables, PIFA could consistently consumes less memory than a dense weight matrix. In contrast, traditional low-rank decomposition may exceed the memory cost of dense matrices when $r > \frac{mn}{m+n}$.

Computational cost of PIFA. We analyze the computational cost of each linear layer for an input batch size b, where $\mathbf{X} \in \mathbb{R}^{n \times b}$. We compute the FLOPs for each method as follows:

- For the dense linear layer $\mathbf{Y} = \mathbf{W}\mathbf{X}$, where $\mathbf{W} \in \mathbb{R}^{m \times n}$ and $\mathbf{X} \in \mathbb{R}^{n \times b}$, the computational cost is $2mnb$ FLOPs.
- For the traditional low-rank layer $\mathbf{Y} = \mathbf{U}\mathbf{V}^{\mathrm{T}}\mathbf{X}$, where $\mathbf{U} \in \mathbb{R}^{m \times r}$ and $\mathbf{V}^{\mathrm{T}} \in \mathbb{R}^{r \times n}$, the computational cost includes: $\mathbf{V}^{\mathrm{T}}\mathbf{X}$ ($2rnb$) and $\mathbf{U}(\mathbf{V}^{\mathrm{T}}\mathbf{X})$ ($2mrb$). The total cost is $2rnb + 2mrb = 2br(m+n)$ FLOPs.
- For the PIFA layer (Algorithm 2), the computational cost includes: $\mathbf{Y}_p \leftarrow \mathbf{W}_p\mathbf{X}$ ($2rnb$) and $\mathbf{Y}_{np} \leftarrow \mathbf{C}\mathbf{Y}_p$ $2br(m-r)$. The total cost is $2rnb + 2br(m-r) = 2br(m+n-r)$ FLOPs.

PIFA's computational cost is proportional to its memory cost, differing only by a factor of $2b$. As a result, PIFA consistently outperforms both dense linear layers and traditional low-rank layers in computational efficiency.

Comparison with LU and QR decomposition. Figure 5 compares the structure of LU and QR decomposition with Pivoting Factorization on a permuted weight matrix, where pivot rows have already been moved to the top. LU decomposition retains the same number of non-trivial parameters (i.e., those not preset as zero or one) as Pivoting Factorization. However, the trapezoidal distribution of non-trivial parameters in LU decomposition complicates efficient storage and computation on the GPU. In contrast, PIFA reorganizes all non-trivial parameters into a rectangular distribution, which is more GPU-friendly for storage and computation. Thus, Pivoting Factorization is more efficient for GPU computation.

B Online Reformulation of the Least Square Solution

Equation 3 requires loading the entire calibration dataset $\mathbf{X}$ into GPU memory to compute the least squares solution. As a result, the number of calibration samples is limited to a maximum of 16 on LLaMA2-7B (4 on LLaMA2-70B) with a 48GB A6000 GPU, leading to overfitting to the calibration data (see Section G).

Applying the associative property of matrix multiplication, we reformulate Equation 3 into its online version:

$$\mathbf{U}_r = \mathbf{W}(\mathbf{X}\mathbf{X}^{\mathrm{T}})\mathbf{V}(\mathbf{V}^{\mathrm{T}}(\mathbf{X}\mathbf{X}^{\mathrm{T}})\mathbf{V})^{-1} \tag{7}$$

The term $\mathbf{X}\mathbf{X}^{\mathrm{T}}$ can be computed incrementally as $\mathbf{X}\mathbf{X}^{\mathrm{T}} = \sum_{i=1}^{b} \mathbf{x}_i\mathbf{x}_i^{\mathrm{T}}$, where $\mathbf{x}_i$ represents the input of sample i. As $\mathbf{X}\mathbf{X}^{\mathrm{T}} \in \mathbb{R}^{n \times n}$, the memory consumption of the online least squares solution remains constant, regardless of the number of calibration samples.

C RECONSTRUCTING $\mathbf{V}^{\mathrm{T}}$

Equation 3 reconstructs only $\mathbf{U}$. We find it beneficial to also update $\mathbf{V}^{\mathrm{T}}$and provide the closed-form solution:

$$\begin{aligned}\mathbf{V}_r^{\mathrm{T}} &= \arg\min_{\mathbf{V}^{\mathrm{T}}} \|\mathbf{Y}_t - \mathbf{U}\mathbf{V}^{\mathrm{T}}\mathbf{X}\|_{\mathrm{F}} \\ &= (\mathbf{U}^{\mathrm{T}}\mathbf{U})^{-1}\mathbf{U}^{\mathrm{T}}\mathbf{Y}_t\mathbf{X}^{\mathrm{T}}(\mathbf{X}\mathbf{X}^{\mathrm{T}})^{-1}\end{aligned} \tag{8}$$

The proof is provided in Appendix D. Updating $\mathbf{V}^{\mathrm{T}}$ can also be performed online by incrementally computing $\mathbf{Y}\mathbf{X}^{\mathrm{T}}$ and $\mathbf{X}\mathbf{X}^{\mathrm{T}}$.

D CLOSED-FORM SOLUTION OF $\mathbf{V}^{\mathrm{T}}$

We aim to prove that minimizing the Frobenius norm $\|\mathbf{Y} - \mathbf{U}\mathbf{V}^{\mathrm{T}}\mathbf{X}\|_F$ with respect to $\mathbf{V}^{\mathrm{T}}$ is equivalent to performing the following two-step optimization:

1. First, minimize $\|\mathbf{Y} - \mathbf{W}\mathbf{X}\|_F$ with respect to $\mathbf{W}$.

2. Then, minimize $\|\mathbf{W} - \mathbf{U}\mathbf{V}^{\mathrm{T}}\|_F$ with respect to $\mathbf{V}^{\mathrm{T}}$.

We begin by directly minimizing $\|\mathbf{Y} - \mathbf{U}\mathbf{V}^{\mathrm{T}}\mathbf{X}\|_F^2$ with respect to $\mathbf{V}^{\mathrm{T}}$.

D.1 DIRECT OPTIMIZATION

$$\begin{aligned}f(\mathbf{V}) &= \|\mathbf{Y} - \mathbf{U}\mathbf{V}^{\mathrm{T}}\mathbf{X}\|_F^2 \\ &= \mathrm{Tr}\left((\mathbf{Y} - \mathbf{U}\mathbf{V}^{\mathrm{T}}\mathbf{X})^{\mathrm{T}}(\mathbf{Y} - \mathbf{U}\mathbf{V}^{\mathrm{T}}\mathbf{X})\right) \\ &= \mathrm{Tr}\left(\mathbf{Y}^{\mathrm{T}}\mathbf{Y} - \mathbf{Y}^{\mathrm{T}}\mathbf{U}\mathbf{V}^{\mathrm{T}}\mathbf{X} - \mathbf{X}^{\mathrm{T}}\mathbf{V}\mathbf{U}^{\mathrm{T}}\mathbf{Y} + \mathbf{X}^{\mathrm{T}}\mathbf{V}\mathbf{U}^{\mathrm{T}}\mathbf{U}\mathbf{V}^{\mathrm{T}}\mathbf{X}\right) \\ &= \mathrm{Tr}(\mathbf{Y}^{\mathrm{T}}\mathbf{Y}) - 2\,\mathrm{Tr}(\mathbf{V}^{\mathrm{T}}\mathbf{X}\mathbf{Y}^{\mathrm{T}}\mathbf{U}) + \mathrm{Tr}(\mathbf{V}^{\mathrm{T}}\mathbf{X}\mathbf{X}^{\mathrm{T}}\mathbf{V}\mathbf{U}^{\mathrm{T}}\mathbf{U})\end{aligned}$$

Let us define intermediate matrices:

$$\begin{aligned}\mathbf{A} &= \mathbf{X}\mathbf{Y}^{\mathrm{T}}\mathbf{U} \\ \mathbf{B} &= \mathbf{X}\mathbf{X}^{\mathrm{T}} \\ \mathbf{C} &= \mathbf{U}^{\mathrm{T}}\mathbf{U}\end{aligned}$$

The objective function becomes:

$$f(\mathbf{V}) = \text{const} - 2\,\mathrm{Tr}(\mathbf{V}^{\mathrm{T}}\mathbf{A}) + \mathrm{Tr}(\mathbf{V}^{\mathrm{T}}\mathbf{B}\mathbf{V}\mathbf{C})$$

where "const" denotes terms independent of $\mathbf{V}$.

Compute the gradient of $f(\mathbf{V})$ with respect to $\mathbf{V}$:

$$\frac{\partial f}{\partial \mathbf{V}} = -2\mathbf{A} + 2\mathbf{B}\mathbf{V}\mathbf{C}$$

Set the gradient to zero:

$$-2\mathbf{A} + 2\mathbf{B}\mathbf{V}\mathbf{C} = 0 \implies \mathbf{B}\mathbf{V}\mathbf{C} = \mathbf{A}$$

Assuming $\mathbf{B}$ and $\mathbf{C}$ are invertible, we solve for $\mathbf{V}$:

$$\mathbf{V} = \mathbf{B}^{-1}\mathbf{A}\mathbf{C}^{-1}$$

Substituting back the definitions of $\mathbf{A}, \mathbf{B}, \mathbf{C}$:

$$\mathbf{V} = (\mathbf{X}\mathbf{X}^{\mathrm{T}})^{-1} \left(\mathbf{X}\mathbf{Y}^{\mathrm{T}}\mathbf{U}\right) (\mathbf{U}^{\mathrm{T}}\mathbf{U})^{-1}$$

Simplify:

$$\mathbf{V}^{\mathrm{T}} = (\mathbf{U}^{\mathrm{T}}\mathbf{U})^{-1}\mathbf{U}^{\mathrm{T}}\mathbf{Y}\mathbf{X}^{\mathrm{T}}(\mathbf{X}\mathbf{X}^{\mathrm{T}})^{-1}$$

D.2 Two-Step Optimization

Now, we perform the two-step optimization and show it leads to the same result.

First, minimize $\|\mathbf{Y} - \mathbf{W}\mathbf{X}\|_F^2$ with respect to $\mathbf{W}$.

Compute the gradient:

$$\frac{\partial}{\partial \mathbf{W}} \|\mathbf{Y} - \mathbf{W}\mathbf{X}\|_F^2 = -2(\mathbf{Y} - \mathbf{W}\mathbf{X})\mathbf{X}^{\mathrm{T}}$$

Set the gradient to zero:

$$(\mathbf{Y} - \mathbf{W}\mathbf{X})\mathbf{X}^{\mathrm{T}} = 0 \implies \mathbf{Y}\mathbf{X}^{\mathrm{T}} = \mathbf{W}\mathbf{X}\mathbf{X}^{\mathrm{T}}$$

Assuming $\mathbf{X}\mathbf{X}^{\mathrm{T}}$ is invertible:

$$\mathbf{W} = \mathbf{Y}\mathbf{X}^{\mathrm{T}}(\mathbf{X}\mathbf{X}^{\mathrm{T}})^{-1}$$

Next, minimize $\|\mathbf{W} - \mathbf{U}\mathbf{V}^{\mathrm{T}}\|_F^2$ with respect to $\mathbf{V}^{\mathrm{T}}$.

Compute the gradient:

$$\frac{\partial}{\partial \mathbf{V}} \|\mathbf{W} - \mathbf{U}\mathbf{V}^{\mathrm{T}}\|_F^2 = -2\mathbf{U}^{\mathrm{T}}(\mathbf{W} - \mathbf{U}\mathbf{V}^{\mathrm{T}})$$

Set the gradient to zero:

$$\mathbf{U}^{\mathrm{T}}\mathbf{W} = \mathbf{U}^{\mathrm{T}}\mathbf{U}\mathbf{V}^{\mathrm{T}}$$

Assuming $\mathbf{U}^{\mathrm{T}}\mathbf{U}$ is invertible:

$$\mathbf{V}^{\mathrm{T}} = (\mathbf{U}^{\mathrm{T}}\mathbf{U})^{-1}\mathbf{U}^{\mathrm{T}}\mathbf{W}$$

Substitute $\mathbf{W}$:

$$\mathbf{V}^{\mathrm{T}} = (\mathbf{U}^{\mathrm{T}}\mathbf{U})^{-1}\mathbf{U}^{\mathrm{T}} \left(\mathbf{Y}\mathbf{X}^{\mathrm{T}}(\mathbf{X}\mathbf{X}^{\mathrm{T}})^{-1}\right)$$

Simplify:

$$\mathbf{V}^{\mathrm{T}} = (\mathbf{U}^{\mathrm{T}}\mathbf{U})^{-1}\mathbf{U}^{\mathrm{T}}\mathbf{Y}\mathbf{X}^{\mathrm{T}}(\mathbf{X}\mathbf{X}^{\mathrm{T}})^{-1}$$

D.3 Conclusion

The solution for $\mathbf{V}^{\mathrm{T}}$ obtained through both the direct optimization and the two-step optimization is:

$$\mathbf{V}^{\mathrm{T}} = (\mathbf{U}^{\mathrm{T}}\mathbf{U})^{-1}\mathbf{U}^{\mathrm{T}}\mathbf{Y}\mathbf{X}^{\mathrm{T}}(\mathbf{X}\mathbf{X}^{\mathrm{T}})^{-1}$$

Therefore, minimizing $\|\mathbf{Y} - \mathbf{U}\mathbf{V}^{\mathrm{T}}\mathbf{X}\|_F$ with respect to $\mathbf{V}^{\mathrm{T}}$ is equivalent to first optimizing $\|\mathbf{Y} - \mathbf{W}\mathbf{X}\|_F$ with respect to $\mathbf{W}$, and then optimizing $\|\mathbf{W} - \mathbf{U}\mathbf{V}^{\mathrm{T}}\|_F$ with respect to $\mathbf{V}^{\mathrm{T}}$.

E EXPERIMENT DETAILS

E.1 MODELS AND DATASETS

We apply MPIFA to pre-trained LLMs: LLaMA2 (7B, 13B, 70B) (Touvron et al., 2023b) and LLaMA3 (8B) (Dubey et al., 2024). Both the calibration data and perplexity (PPL) evaluation are based on the WikiText2 dataset (Merity et al., 2022).

E.2 COMPARISON WITH LOW-RANK PRUNING

We evaluate MPIFA against state-of-the-art low-rank pruning methods: ASVD (Yuan et al., 2023) and SVD-LLM (Wang et al., 2024). Vanilla SVD is also included for reference. SVD-LLM has two versions, as detailed in their original paper. Following their approach, we select the best-performing version for each density. Results for both versions of SVD-LLM are provided in Table 7. MPIFA utilizes 128 calibration samples and sets $\lambda = 0.25$. For all models except LLaMA-2-70B, MPIFA reconstructs both $\mathbf{U}$ and $\mathbf{V}^{\mathrm{T}}$. For LLaMA-2-70B, MPIFA reconstructs only $\mathbf{U}$.

E.3 COMPARISON WITH SEMI-STRUCTURED PRUNING

We further compare MPIFA with 2:4 semi-structured pruning methods: magnitude pruning (Zhu & Gupta, 2017), and two recent state-of-the-art works Wanda (Sun et al., 2024), and RIA (Zhang et al., 2024). According to (Mishra et al., 2021), for 16-bit operands, 2:4 sparse leads to $\sim$44% savings in GPU memory. Therefore, we compare 2:4 sparse method with MPIFA at 0.55 density to ensure that all methods achieve the same memory reduction (see Table 4 for memory comparison).

E.4 MPIFA

We combine Online Error-Accumulation-**M**inimization Reconstruction with **Pi**voting **Fa**ctorization into an end-to-end low-rank compression method, **MPIFA** (illustrated in Figure 2). MPIFA proceeds as follows: ① First, Online Error-Accumulation-Minimization Reconstruction iis applied to obtain and refine the low-rank matrices $\mathbf{U}_r$ and $\mathbf{V}_r^{\mathrm{T}}$; ② Then, PIFA decomposes the singular matrix $\mathbf{W}' = \mathbf{U}_r\mathbf{V}_r^{\mathrm{T}}$ into $\mathcal{I}, \mathbf{W}_p, \mathbf{C} \leftarrow \mathrm{PIFA}(\mathbf{W}')$, which are stored in a PIFA layer that replaces the original linear layer.

The full method of MPIFA is outlined in Algorithm 3.

Algorithm 3 MPIFA

input Original weight matrix $\mathbf{W} \in \mathbb{R}^{m\times n}$; calibration input from dense $\mathbf{X}_o \in \mathbb{R}^{n\times b}$; calibration input from low rank $\mathbf{X}_u \in \mathbb{R}^{n\times b}$; target rank r; original output ratio λ

Part 1: Online Error-Accumulation-Minimization Reconstruction

Compute dense output as dense input of next module: $\mathbf{Y}_o = \mathbf{W}\mathbf{X}_o$
Use SVD-LLM's pruning (truncation-aware data whitening) to convert to low-rank matrix: $\mathbf{U}, \mathbf{V}^{\mathrm{T}} \leftarrow \text{SVD-LLM}(\mathbf{W})$
Compute $\mathbf{X}\mathbf{X}^{\mathrm{T}}$ accumulatively: $\mathbf{X}\mathbf{X}^{\mathrm{T}} \leftarrow \sum_{i=1}^{b} \mathbf{x}_u^i {\mathbf{x}_u^i}^{\mathrm{T}}$
Compute $\mathbf{Y}_t\mathbf{X}^{\mathrm{T}}$ accumulatively: $\mathbf{Y}_t\mathbf{X}^{\mathrm{T}} \leftarrow \sum_{i=1}^{b} (\lambda\mathbf{W}\mathbf{x}_o^i + (1-\lambda)\mathbf{W}\mathbf{x}_u^i){\mathbf{x}_u^i}^{\mathrm{T}}$
Reconstruct $\mathbf{U}$ as $\mathbf{U}_r$: $\mathbf{U}_r \leftarrow (\mathbf{Y}_t\mathbf{X}^{\mathrm{T}})\mathbf{V}(\mathbf{V}^{\mathrm{T}}(\mathbf{X}\mathbf{X}^{\mathrm{T}})\mathbf{V})^{-1}$
Reconstruct $\mathbf{V}$ as $\mathbf{V}_r$: $\mathbf{V}_r^{\mathrm{T}} \leftarrow (\mathbf{U}_r^{\mathrm{T}}\mathbf{U}_r)^{-1}\mathbf{U}_r^{\mathrm{T}}(\mathbf{Y}_t\mathbf{X}^{\mathrm{T}})(\mathbf{X}\mathbf{X}^{\mathrm{T}})^{-1}$
Compute low-rank output as low-rank input of next module: $\mathbf{Y}_u = \mathbf{W}\mathbf{X}_u$

Part 2: PIFA

Compute low-rank matrix $\mathbf{W}'$: $\mathbf{W}' \leftarrow \mathbf{U}_r\mathbf{V}_r^{\mathrm{T}}$
Use Algorithm 1 to build the PIFA layer P using low-rank matrix $\mathbf{W}'$

output PIFA layer P

A potential issue is that $\mathbf{X}\mathbf{X}^{\mathrm{T}}$ can be singular in some cases, leading to NaN values when calculating the inverse matrix during $\mathbf{V}$ reconstruction. To address this, we leverage prior knowledge that $\mathbf{U}\mathbf{V}^{\mathrm{T}}$

should approximate $\mathbf{W}$ by adding a regularization term to the original optimization target, modifying Equation 8 as follows:

$$\begin{aligned}\mathbf{V}_r^{\mathrm{T}} &= \arg\min_{\mathbf{V}^{\mathrm{T}}} \|\mathbf{Y}_t - \mathbf{U}\mathbf{V}^{\mathrm{T}}\mathbf{X}\|_{\mathrm{F}} + \alpha\|\mathbf{W} - \mathbf{U}\mathbf{V}^{\mathrm{T}}\|_{\mathrm{F}} \\ &= (\mathbf{U}^{\mathrm{T}}\mathbf{U})^{-1}\mathbf{U}^{\mathrm{T}}(\mathbf{Y}_t\mathbf{X}^{\mathrm{T}} + \alpha\mathbf{W})(\mathbf{X}\mathbf{X}^{\mathrm{T}} + \alpha\mathbf{I})^{-1}\end{aligned} \tag{9}$$

where α is the regularization coefficient, set to 0.001 in all experiments. Regularization is unnecessary for reconstructing $\mathbf{U}$, as no singularity issues were observed for $\mathbf{V}^{\mathrm{T}}(\mathbf{X}\mathbf{X}^{\mathrm{T}})\mathbf{V}$.

E.5 MPIFA$_{\mathrm{NS}}$

MPIFA$_{\mathrm{NS}}$ is the non-uniform sparsity variant of MPIFA, designed to leverage different sparsity distributions across model layers and module types for improved performance. It employs 512 calibration samples. This approach incorporates two key components to define module densities: **Type Density** and **Layer Density**, which are combined multiplicatively to determine the final density for each module.

Type Density. Type Density introduces non-uniform sparsity between attention and MLP modules. Based on insights from prior literature (Yuan et al., 2023), MLP modules exhibit higher sensitivity to pruning compared to attention modules. To account for this, we search for the density of attention modules within $\{\text{Global Density}, \text{Global Density} - 1\}$, optimizing for performance. The density of MLP modules is then calculated to ensure that the model's global density remains unchanged.

Layer Density. Layer Density accounts for non-uniform sparsity across layers. For this, MPIFA$_{\mathrm{NS}}$ adopts the layerwise density distribution from OWL (Yin et al.), which identifies layer-wise densities based on outlier distribution. By directly utilizing these precomputed layer densities, MPIFA$_{\mathrm{NS}}$ ensures that density is allocated more effectively across layers, balancing pruning across regions of varying importance.

Final Module Density. The final density for each module in MPIFA$_{\mathrm{NS}}$ is calculated as:

$$\text{Module Density} = \frac{\text{Type Density} \times \text{Layer Density}}{\text{Global Density}}.$$

This formulation ensures that the final density for each module accounts for both type- and layer-specific sparsity requirements, leading to a more effective pruning configuration optimizing performance while maintains the global density same.

In summary, MPIFA$_{\mathrm{NS}}$ combines the benefits of non-uniform sparsity across both types of modules and individual layers, achieving better performance while ensuring the global density of the model remains unchanged.

E.6 MPIFA$_{\mathrm{NS}}$ FINE-TUNING

We investigate how fine-tuning helps recover the performance loss caused by low-rank pruning. Fine-tuning is performed using a mixed dataset comprising the training set of WikiText2 and one shard (1/1024) of the training set of C4 (Raffel et al., 2020). WikiText2's training set is more aligned with the evaluation dataset but contains a limited number of tokens, whereas the C4 dataset is significantly larger but less aligned with the test set. To balance these characteristics, the datasets are mixed at a ratio of 2% WikiText2 to 98% C4.

We limit fine-tuning to a single epoch, which requires approximately one day on a single GPU (around 1000 steps). The fine-tuning process updates all pruned parameters, including low-rank matrices and semi-sparse matrices, while keeping other parameters, such as embeddings, fixed.

The learning rate is set to 3×10^{-6}, with a warmup phase covering the first 5% of total steps, followed by a linear decay to zero. The sequence length is fixed at 1024, with a batch size of 1 and gradient accumulation steps of 128.

As shown in Table 5, fine-tuned MPIFA$_{NS}$ achieves the best performance among all fine-tuned pruning methods, bringing its perplexity close to the dense baseline at 55% density. Unlike semi-structured methods, which cannot accelerate the backward pass due to transposed weight tensors violating the 2:4 constraint (Mishra et al., 2021), PIFA and other low-rank methods enable acceleration in both the forward and backward passes.

Table 5: **Perplexity (↓) of pruned models after fine-tuning** on WikiText2 (LLaMA2-7B). The best-performance pruning method is indicated in **bold**.

Method	LLaMA2-7B
Dense	5.47
Magnitude 2:4	6.63
Wanda 2:4	6.40
RIA 2:4	6.37
SVD 55%	9.24
ASVD 55%	8.64
SVD-LLM 55%	7.36
MPIFA$_{NS}$ 55%	**6.34**

Table 6: **End-to-end efficiency of MPIFA$_{NS}$** on LLaMA2 models, on FP16 (FP32 isn't supported by semi-sparse). The highest throughput and lowest memory are indicated in **bold**. MPIFA$_{NS}$ consistently outperforms semi-sparse in both throughput and memory with 55% density. †Enabling KV cache for semi-sparse model will cause `SparseSemiStructuredTensorCUSPARSELT only supports a specific set of operations, can't perform requested op (expand.default)`

Model	Metrics	GPU	Use KV Cache	Dense	2:4 (cuSPARSELt)	2:4 (CUTLASS)	MPIFA$_{NS}$ 55%
llama2-7b	Throughput (token/s)	A6000	No	354.9	306.6	327.5	**472.6**
			Yes	3409	Error†	Error	**4840**
		A100	No	614.8	636.2	582.3	**822.2**
			Yes	6918	Error	Error	**7324**
	Memory (GB)			12.55	7.274	7.290	**7.174**
llama2-13b	Throughput (token/s)	A6000	No	190.0	163.2	180.0	**268.7**
			Yes	2156	Error	Error	**2721**
		A100	No	345.4	362.4	321.5	**473.3**
			Yes	4217	Error	Error	**4532**
	Memory (GB)			24.36	13.90	13.99	**13.69**

F END-TO-END LLM INFERENCE.

Table 6 compares the end-to-end inference throughput and memory usage of MPIFA$_{NS}$ with semi-sparsity (2:4 cuSPARSELt and CUTLASS) on LLaMA2-7B and LLaMA2-13B models in FP16. MPIFA$_{NS}$ consistently outperforms semi-sparsity in both throughput and memory efficiency at 55% density. Furthermore, the operations supported by semi-sparsity are limited in `torch.sparse`, resulting in errors when the KV cache is enabled, which further limits the application of semi-sparse for LLM inference.

G ABLATION STUDY

Impact of PIFA and M Table 7 presents an ablation study that evaluates the impact of our Online Error-Accumulation-Minimization Reconstruction (denoted as M) and Pivoting Factorization (PIFA) on perplexity across varying parameter densities. The methods compared include:

- **W:** Using only the pruning step of SVD-LLM (truncation-aware data whitening).
- **W + U:** Applying SVD-LLM's pruning followed by full-batch reconstruction.

Table 7: **Ablation: Impact of PIFA and M on perplexity (↓) across parameter densities.** (the proportion of parameters remaining compared with the original model) on WikiText2. W denotes using SVD-LLM's pruning (truncation-aware data whitening) only; W + U denotes using SVD-LLM's pruning and full-batch reconstruction; W + M denotes using our Online Error-Accumulation-Minimization Reconstruction, which incorporates SVD-LLM's pruning as the initial step; W + M + PIFA denotes using Online Error-Accumulation-Minimization Reconstruction followed by PIFA, i.e., MPIFA. The best performance method is indicated in **bold**.

		Density						
Model	Method	100%	90%	80%	70%	60%	50%	40%
LLaMA2-7B	W	5.47	7.27	8.38	10.66	16.14	33.27	89.98
	W + U		7.60	8.84	11.15	16.11	27.19	54.20
	W + M		6.71	7.50	8.86	11.45	16.55	25.26
	W + M + PIFA (MPIFA)		**5.69**	**6.16**	**7.05**	**8.81**	**12.77**	**21.25**
LLaMA2-13B	W	4.88	5.94	6.66	8.00	10.79	18.38	43.92
	W + U		6.45	7.37	9.07	12.52	20.95	42.79
	W + M		5.80	6.41	7.42	9.31	13.09	19.93
	W + M + PIFA (MPIFA)		**5.03**	**5.39**	**7.12**	**7.41**	**10.30**	**16.72**
LLaMA2-70B	W	3.32	4.12	4.58	5.31	6.60	9.09	14.82
	W + U		8.23	8.33	8.66	10.02	13.41	22.39
	W + M		4.15	4.63	5.31	6.46	8.72	14.11
	W + M + PIFA (MPIFA)		**3.54**	**3.96**	**4.58**	**5.54**	**7.40**	**12.01**
LLaMA3-8B	W	6.14	9.83	13.62	25.43	76.86	290.3	676.7
	W + U		10.63	14.66	23.66	42.60	83.46	163.5
	W + M		9.16	11.25	15.27	23.55	36.14	53.85
	W + M + PIFA (MPIFA)		**6.93**	**8.31**	**10.83**	**16.41**	**28.90**	**47.02**

- **W + M:** Employing our Online Error-Accumulation-Minimization Reconstruction, which incorporates SVD-LLM's pruning as the initial step.
- **W + M + PIFA:** Combining Online Error-Accumulation-Minimization Reconstruction with PIFA (denoted as MPIFA).

The results reveal several key findings:

1. **Full-batch reconstruction (W + U) occasionally worsens perplexity compared to using only the pruning step (W).** This highlights the drawbacks of full-batch methods, as overfitting to the limited calibration data can degrade performance.
2. **Our reconstruction method (W + M) consistently outperforms full-batch reconstruction (W + U) and pruning alone (W) across all models and densities.** This demonstrates the effectiveness of Online Error-Accumulation-Minimization Reconstruction in reducing error accumulation and improving the compression of low-rank matrices.
3. **PIFA further improves performance when combined with M.** The W + M + PIFA configuration achieves the best perplexity across all settings, validating the advantage of applying PIFA for additional parameter reduction without inducing any additional loss.

These findings emphasize the significance of M and PIFA in achieving superior low-rank pruning performance.

Impact of mix ratio λ in M. The mix ratio λ in Equation 5 determines the proportion of the dense data flow in the reconstruction target. As shown in Figure 6, using a moderate ratio $\lambda = 0.25$, MPIFA achieves significantly lower PPL compared to $\lambda = 0$, where the reconstruction target relies solely on the low-rank data flow, as in previous studies (Wang et al., 2024; Frantar & Alistarh, 2023) did. This demonstrates the effectiveness of our error-accumulation-corrected strategy, in which the dense data flow output is beneficial as part of the reconstruction target. In Figure 6, we also observe that an excessively large λ increases PPL, indicating overfitting to the calibration data.

Impact of Calibration Sample Size. M depends on calibration data to accurately estimate $\mathbf{U}$ and $\mathbf{V}^{\mathrm{T}}$. As shown in Figure 7, the perplexity of MPIFA decreases as the number of calibration samples increases. We hypothesize that increasing the number of calibration samples reduces the condition number of the least squares solution, improving numerical stability.

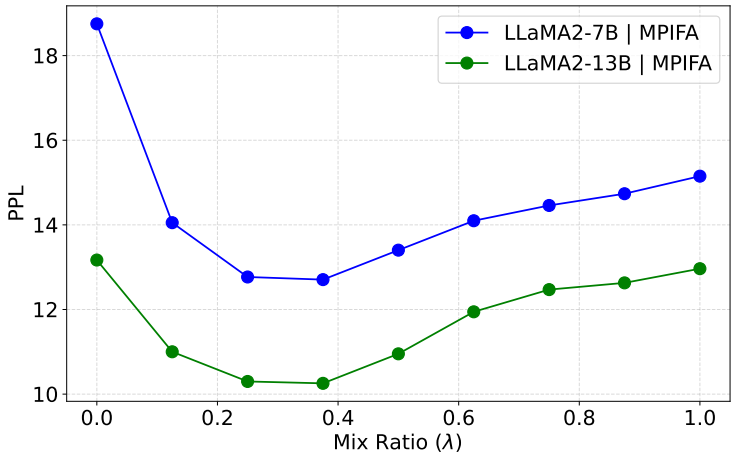

Figure 6: **Impact of mix ratio.** With 0.5 density, MPIFA achieves lowest PPL when the mix ratio λ in Equation 5 is around 0.25.

Table 8: **C4 Perplexity (↓) at different parameter density** (proportion of remaining parameters relative to the original model). The best-performing method is highlighted in **bold**.

			Density					
Model	Method	100%	90%	80%	70%	60%	50%	40%
LLaMA2-7B	SVD	7.29	18931	27154	37208	56751	58451	70567
	ASVD		**7.98**	12.46	201.0	9167	25441	24290
	SVD-LLM		13.95	19.89	33.02	61.97	129.8	262.9
	MPIFA		8.15	**10.20**	**14.68**	**25.43**	**52.01**	**97.71**
LLaMA2-13B	SVD	6.74	1994	6301	37250	22783	18196	84680
	ASVD		**7.15**	9.30	23.54	468.5	3537	3703
	SVD-LLM		10.93	14.99	24.44	46.65	110.4	267.8
	MPIFA		7.27	**8.79**	**21.00**	**21.33**	**42.03**	**80.47**
LLaMA2-70B	SVD	5.74	10.16	23.28	121.4	1659	7045	12039
	ASVD		OOM	OOM	OOM	OOM	OOM	OOM
	SVD-LLM		7.12	8.71	12.21	21.40	44.10	103.3
	MPIFA		**6.00**	**6.76**	**8.67**	**13.60**	**29.04**	**63.38**
LLaMA3-8B	SVD	9.47	323597	461991	172968	70896	143573	271176
	ASVD		**14.43**	272.1	8511	18701	108117	9466
	SVD-LLM		38.54	98.65	223.5	460.0	784.8	1416
	MPIFA		14.76	**22.45**	**44.62**	**123.0**	**257.4**	**429.2**

To investigate this, we calculate the condition numbers of $\mathbf{V}^{\mathrm{T}}\mathbf{X}\mathbf{X}^{\mathrm{T}}\mathbf{V}$ in Equation 7 and $\mathbf{X}\mathbf{X}^{\mathrm{T}}$ in Equation 8, as their inverses are required for reconstructing $\mathbf{U}$ and $\mathbf{V}^{\mathrm{T}}$. Figure 8 presents the condition numbers for these matrices in the first layer of LLaMA2-7B. The observed reduction in condition number indicates that the matrices become less singular as the calibration sample size increases, thereby improving numerical stability when solving the least squares equations. This increased stability ultimately results in lower perplexity in the reconstructed model.

Impact of reconstructing $\mathbf{U}$ and $\mathbf{V}^{\mathrm{T}}$. Figures 7a and 7b compare the effects of reconstructing only $\mathbf{U}$, only $\mathbf{V}^{\mathrm{T}}$, and both $\mathbf{U}$ and $\mathbf{V}^{\mathrm{T}}$ across different calibration sizes. The results indicate that with sufficient calibration samples, reconstructing both $\mathbf{U}$ and $\mathbf{V}^{\mathrm{T}}$ achieves lower perplexity than reconstructing only $\mathbf{U}$ or only $\mathbf{V}^{\mathrm{T}}$.

H C4 Perplexity Evaluation

To expand beyond WikiText2, we evaluate all methods on the C4 dataset (Raffel et al., 2020). Table 8 demonstrates that MPIFA significantly outperforms other low-rank pruning methods across all model sizes and compression densities.

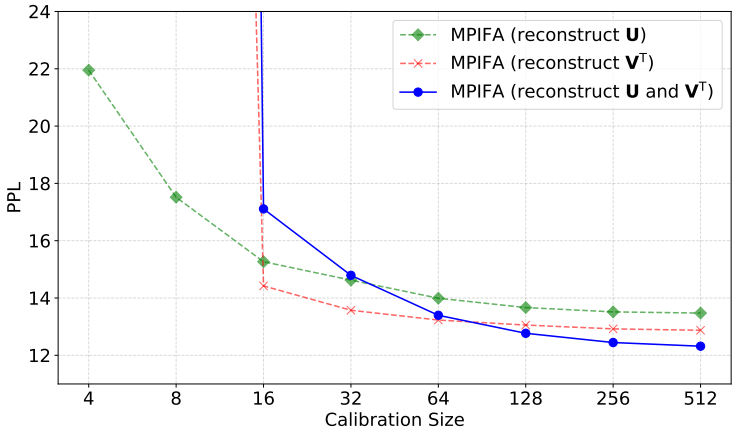

(a) LLaMA2-7B

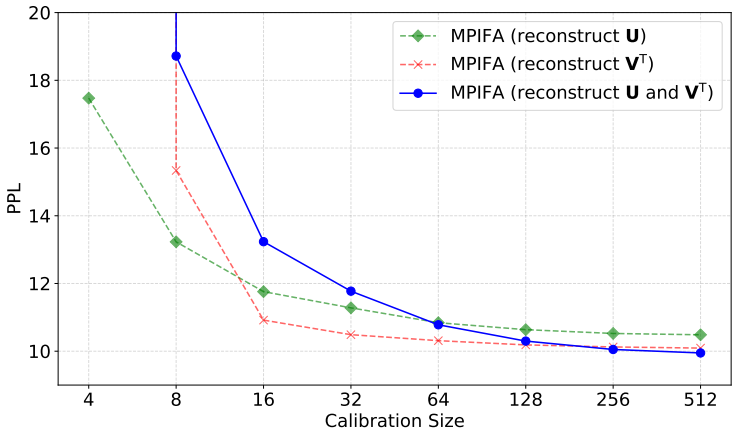

(b) LLaMA2-13B

Figure 7: **Impact of calibration sample size.** On MPIFA with 0.5 density, reconstructing both $\mathbf{U}$ and $\mathbf{V}^{\mathrm{T}}$ is more sensitive to the number of calibration samples than reconstructing only $\mathbf{U}$.

I Zero-Shot Evaluation

We also evaluate MPIFA on downstream LLM tasks using the SuperGLUE benchmark at Table 9. We report zero-shot accuracy across multiple compression ratios on LLaMA2-7B. We run the experiments with the public GitHub benchmark EleutherAI/lm-evaluation-harness (Gao et al., 2021). Results show that MPIFA achieves the best mean accuracy across all densities.

J Related Work

J.1 Connection-wise pruning

Pruning methods We define connection-wise pruning as removing certain connections between neurons in the network that are deemed less important. To achieve this, a series of methods have been proposed. Optimal Brain Damage (OBD) (Le Cun et al., 1990) and Optimal Brain Surgeon (OBS) (Hassibi et al., 1993) were proposed to identify the weight saliency by computing the Hessian matrix using calibration data. Recent methods such as SparseGPT (Frantar & Alistarh, 2023), Wanda (Sun et al., 2024), RIA (Zhang et al., 2024), along with other works (Fang et al., 2024; Dong et al., 2024; Das et al., 2024), have advanced these ideas. Wanda prunes weights with the smallest magnitudes multiplied by input activations. Relative Importance and Activations (RIA) jointly considers both the input and output channels of weights along with activation information. Furthermore, OWL (Yin

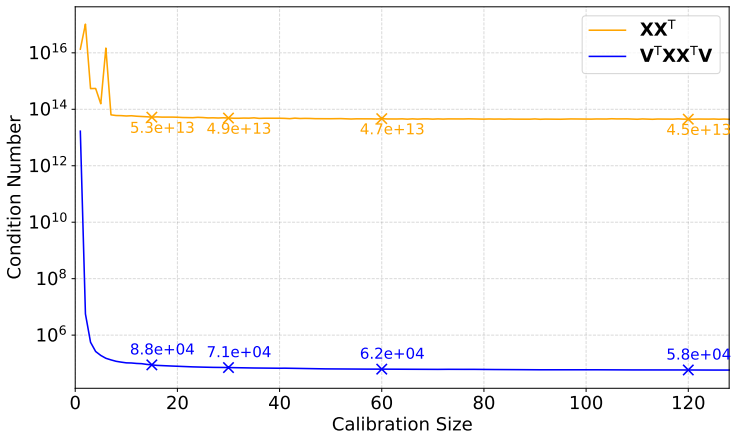

Figure 8: **Condition number.** Condition numbers of $\mathbf{V}^T\mathbf{X}\mathbf{X}^T\mathbf{V}$ (Equation 7) and $\mathbf{X}\mathbf{X}^T$ (Equation 8) for the first layer of LLaMA2-7B, whose inverses are used in reconstructing $\mathbf{U}$ and $\mathbf{V}^T$. Larger calibration sizes reduce condition numbers, enhancing numerical stability and lowering perplexity.

Table 9: **Zero-shot evaluations** on SuperGLUE datasets at different parameter density on LLaMA2-7B. All tasks are evaluated using accuracy (↑). The best-performing method is highlighted in **bold**.

Density	Method	BoolQ	CB	COPA	MultiRC	ReCoRD	RTE	WIC	WSC	**Mean**
100%	Dense	77.7	42.9	87.0	57.0	91.6	63.2	49.7	36.5	63.2
90%	SVD	42.6	39.3	67.0	51.0	16.4	55.6	**49.8**	**62.5**	48.0
	ASVD	55.9	37.5	69.0	47.1	42.5	53.4	**49.8**	41.3	49.6
	SVD-LLM	49.1	41.1	79.0	**57.1**	87.8	52.7	48.0	48.1	57.8
	MPIFA	**74.4**	**64.3**	**86.0**	56.7	**91.2**	**58.5**	49.7	36.5	**64.7**
80%	SVD	45.9	**57.1**	59.0	48.9	12.5	47.3	50.0	58.7	47.4
	ASVD	41.6	33.9	58.0	46.8	24.6	**55.2**	50.0	**60.6**	46.3
	SVD-LLM	44.2	41.1	79.0	55.7	84.7	53.1	**50.6**	57.7	58.3
	MPIFA	**69.4**	41.1	**83.0**	**55.8**	**90.3**	53.4	48.7	36.5	**59.8**
70%	SVD	40.2	**46.4**	62.0	43.1	12.4	**53.8**	48.9	**63.5**	46.3
	ASVD	39.2	**46.4**	59.0	48.2	14.0	49.1	**50.3**	**63.5**	46.2
	SVD-LLM	44.4	39.3	**82.0**	44.6	79.8	**53.8**	48.9	60.6	56.7
	MPIFA	**64.8**	41.1	80.0	**57.2**	**87.5**	**53.8**	49.1	42.3	**59.5**
60%	SVD	45.5	**41.1**	61.0	**49.4**	11.4	51.6	50.0	60.6	46.3
	ASVD	48.9	37.5	59.0	46.6	15.2	50.2	50.0	40.4	43.5
	SVD-LLM	38.5	39.3	71.0	44.9	66.4	53.4	50.2	59.6	52.9
	MPIFA	**56.6**	35.7	**79.0**	44.5	**82.8**	**57.8**	**52.0**	**63.5**	**59.0**
50%	SVD	38.6	**44.6**	63.0	43.0	10.1	**52.7**	**50.2**	**63.5**	45.7
	ASVD	**42.2**	39.3	63.0	**45.7**	14.4	**52.7**	50.0	**63.5**	46.3
	SVD-LLM	37.9	41.1	66.0	42.8	50.5	**52.7**	50.0	**63.5**	50.5
	MPIFA	38.0	35.7	**70.0**	42.8	**71.1**	52.4	50.0	**63.5**	**52.9**
40%	SVD	**49.5**	**42.9**	61.0	**48.1**	11.3	52.0	**50.0**	49.0	45.5
	ASVD	42.6	**42.9**	59.0	47.7	14.5	53.1	**50.0**	**64.4**	46.8
	SVD-LLM	37.8	41.1	67.0	42.8	37.0	52.7	**50.0**	63.5	49.0
	MPIFA	37.8	37.5	**68.0**	42.8	**54.7**	**53.8**	**50.0**	63.5	**51.0**

et al.) explores non-uniform sparsity by pruning based on the distribution of outlier activations, while other works (Lu et al., 2024; Mocanu et al., 2018; Ye et al., 2020; Zhuang et al., 2018) investigate alternative criteria for non-uniform sparsity.

Pruning granularity (compared in Table 1):

1. **Unstructured pruning** removes individual weights based on specific criteria. Today, unstructured pruning is a critical technique for compressing large language models (LLMs) to balance performance and computational efficiency. However, unstructured pruning can only accelerate computations on CPUs due to its unstructured sparsity pattern.
2. **Semi-structured pruning**, i.e., N:M sparsity, enforces that in every group of M consecutive elements, N must be zeroed out. This constraint is hardware-friendly and enables optimized

acceleration on GPUs like NVIDIA's Ampere architecture (Mishra et al., 2021). However, semi-structured pruning is constrained by its sparsity pattern, preventing flexible density adjustments and making it inapplicable for acceleration on general GPUs.

3. **Structured pruning** (Ma et al., 2023; van der Ouderaa et al., 2024; Ashkboos et al., 2024; Lin et al., 2024) removes entire components of the model, such as neurons, channels, or attention heads, rather than individual weights. This method preserves tensor alignment and coherence, ensuring compatibility with all GPUs and enabling significant acceleration on both CPUs and GPUs. However, in LLMs, structured pruning can lead to greater loss compared to unstructured or semi-structured pruning.

J.2 Low-rank pruning

Low-rank pruning applies matrix decomposition techniques, such as Singular Value Decomposition (SVD), to approximate weight matrices with lower-rank representations, thereby reducing both storage and computational demands. This approach, compatible with any GPU, represents large matrices as products of smaller ones, improving computational efficiency. Recent studies (Hsu et al., 2022; Yuan et al., 2023; Wang et al., 2024; jai, 2024) highlight the effectiveness of low-rank decomposition in compressing LLMs. However, despite their flexibility, these methods lag behind semi-structured pruning in performance, often leading to a $\mathbf{2}\times$ increase in perplexity (PPL) at the same densities.